Thermoelectric performance of Tellurium-reduced quaternary *p*-type lead-chalcogenide composites

Sima Aminorroaya Yamini[1]*, Heng Wang[2] , Zachary M. Gibbs[3] , Yanzhong Pei[4] , David R.G.Mitchell[5] , Shi Xue Dou[1] and G Jeffrey Snyder[2,5]*

[1] *Australian Institute for Innovative Materials (AIIM), Innovation Campus, University of Wollongong, NSW 2519, Australia.*

[2] *Materials Science, California Institute of Technology, Pasadena, CA 91125, USA.*

[3] *Division of Chemistry and Chemical Engineering, California Institute of Technology, Pasadena, CA 91125, USA.*

[4] *School of Materials Science and Engineering, Tongji University, 4800 Caoan Road, Shanghai 201804, China.*

[5] *Electron Microscopy Centre (EMC), Australian Institute for Innovative Materials (AIIM), Innovation Campus, University of Wollongong, NSW 2519, Australia.*

[6] *ITMO University, Saint Petersburg, Russia.*

Phase diagram and precipitation

Ternary PbTe-PbSe and PbSe-PbS systems show solid solutions over the entire composition range. [1] Whereas, the components of the PbTe-PbS system show very limited solubility with respect to each other, and phase separation of PbS precipitates in the PbTe matrix at the PbTe-rich side of the phase diagram occurs via nucleation and growth (Figure S1). This behaviour is also well understood in the quaternary system of $(PbTe)_{(1-x-y)}(PbSe)_y(PbS)_x$, where addition of PbSe shifts the upper curve of the miscibility gap to lower temperatures [2], as illustrated by the red line in Figure S1 for 10 at% PbSe ($(PbTe)_{(0.9-x)}(PbSe)_{0.1}(PbS)_x$). The final composite contains two phases: PbTe-rich (matrix) and PbS-rich (precipitates) of PbTe(Se,S) and PbS(Se,Te) respectively, and the solubility limit of PbS-rich precipitates is increased in the matrix.

The lever rule was adopted to calculate the fraction of secondary phases at various temperature tielines. The fraction of precipitates in the matrix for $((PbTe)_{0.65}(PbSe)_{0.1}(PbS)_{0.25}$ alloy was calculated to be ~ 14.5 at% and 4.8 at% at 500˚C and 580 ˚C respectively. This indicates that the secondary phase dissolves partially in the matrix during transport properties measurement at high temperatures.

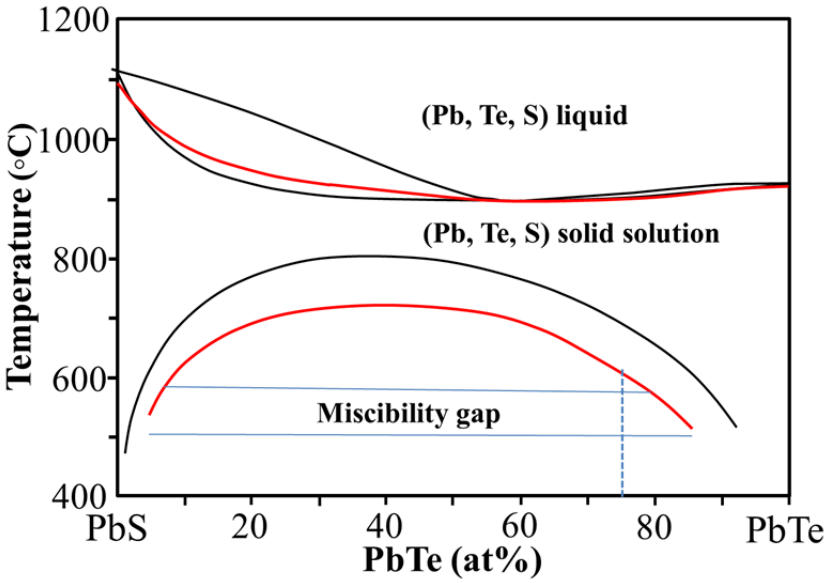

Figure S1: The quasi-binary PbS-PbTe phase diagram (data points extracted from Reference [1]). The red curves show the upper limit of the miscibility gap and solidus curve for $PbSe_{0.1}S_xTe_{(0.9-x)}$ alloys, which indicates that addition of 10 at% PbSe to $PbS_xTe_{(1-x)}$ alloy (red curve) increases PbS solubility in the matrix and shifts the nucleation temperature of the secondary phase to lower temperatures. Blue tie lines have been used to calculate the fraction of secondary phases for $PbSe_{0.1}S_{0.25}Te_{0.75}$ alloy at 500˚C and 580 ˚C.

TEM analyses

The Transmission Electron Microscope (TEM) micrographs of the sintered sample S15 presented in Figure S2(a-c) illustrates the morphology and distribution of submicron precipitates throughout the matrix. Precipitates were characterised using electron diffraction and energy dispersive spectroscopy. Figures S2(d) demonstartes the electron diffraction pattern from [112] zone axis. Selected Area Diffraction patterns included matrix and a single precipitate in Figure S2 (c).

Lead chalcogenides, PbTe, PbSe and PbS have the same crystal structure, with all possessing a halite structure with space group Fm-3m. The lattice parameter of the PbS = 0.5396 nm differs slightly from PbTe = 0.6454 nm. It is therefore anticipated that these isomorphic phases would exhibit a cube//cube orientation relationship. Since the diffraction pattern is a section through reciprocal space, the distance from a diffraction spot to the transmitted beam is inversely related to the interplanar spacing giving rise to it. The tellurium-rich matrix lattice is larger than than of precipitates, therefore, reflections arising from the matrix appear closer to the transmitted beam in all patterns.

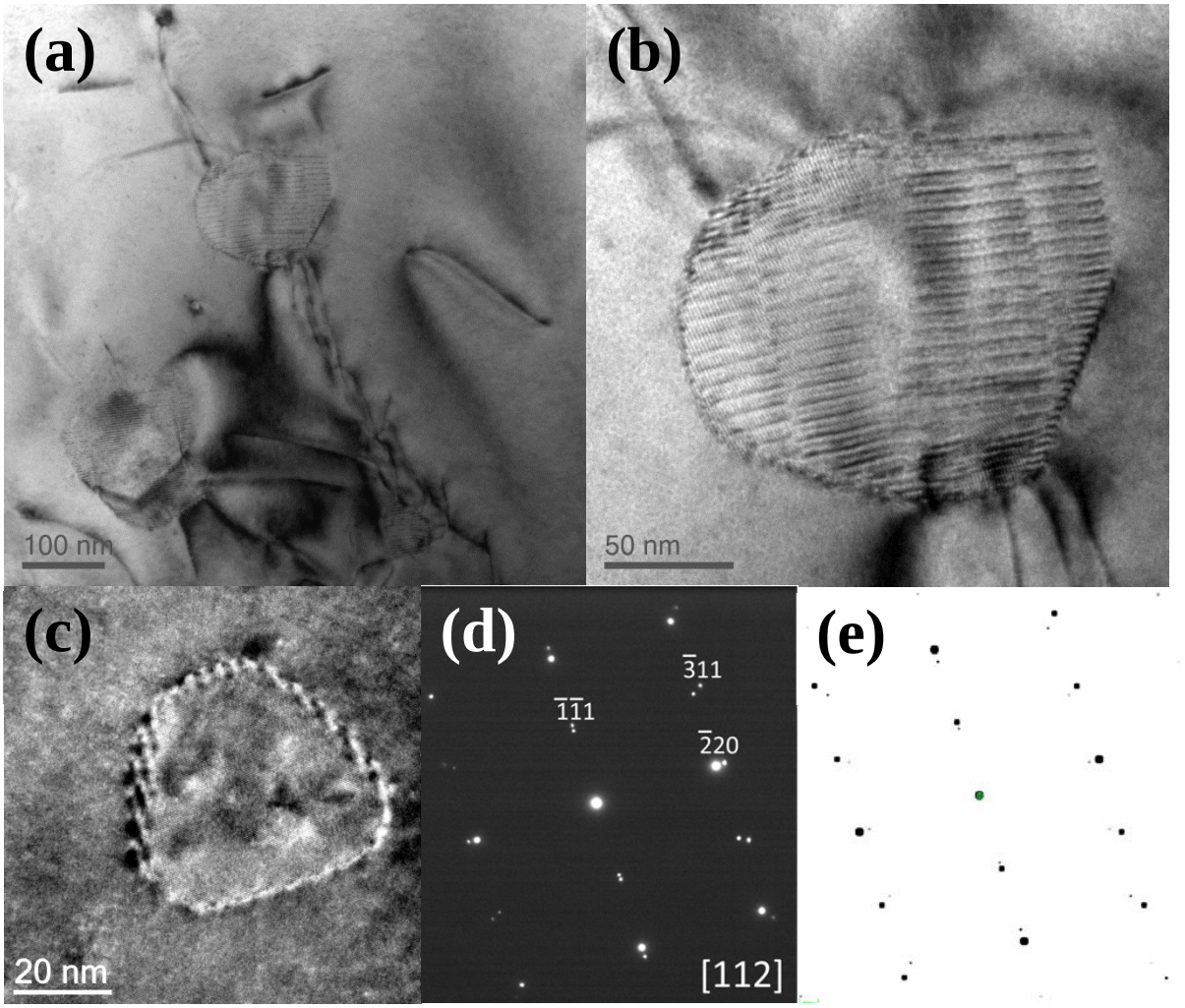

Figure S2: (a-c) TEM micrograph of sulphur-rich precipitates in the tellurium-rich matrix in the $PbS_{0.15}Se_{0.1}Te_{0.75}$; (d) Electron diffraction pattern obtained from an apperture including the precipitate and matrix in Figure S2(c). For each pair of reflections, that closest to the transmitted beam arises from PbTe, which has a larger lattice constant than PbS.

Thermal conductivity

The thermal conductivity κ of samples are calculated from $\kappa = \rho D_T C_p$. The laser flash method (Netzsch LFA457) was used to measure thermal diffusivity D_T. Density, ρ, was calculated using the measured weight and dimensions, and the specific heat capacity, Cp, was estimated by [2]:

$Cp(k_B \text{ per atom}) = 3.07 + 4.7 \times 10^{-4} \times (T/K - 300)$.

The temperature dependence of the measured thermal diffusivity, D_T, and calculated Cp are shown in Figure S5 (a) and (b) respectively.

The lattice thermal conductivity, κ_L, was obtained by subtracting the electronic component, κ_e. The value of charge carrier thermal conductivity κ_e can be determined via Widemann-Franz relation, $\kappa_e = LT/\rho$. where ρ is the resistivity, and L is the Lorenz number estimated as a function of temperature, through fitting the reduced chemical potential η obtained from the Seebeck coefficient, S, as expressed in equation 1. The acoustic phonon scattering and single parabolic band (SPB) model [3] was assumed for this calculation.

$$S = \frac{k}{e}\left(\frac{2F_1(\eta)}{F_0(\eta)} - \eta\right) \tag{1}$$

Where the Fermi integrals F_j are:

$$F_j(\eta) = \int_0^\infty f\varepsilon^j d\varepsilon = \int_0^\infty \frac{\varepsilon^j d\varepsilon}{1+\exp(\varepsilon - \eta)} \tag{2}$$

The η values that fit the temperature dependant S is used to calculate L through equation 3:

$$L = \left(\frac{k}{e}\right)\frac{3F_0(\eta)F_2(\eta) - 4F_1(\eta)^2}{F_0(\eta)^2} \tag{3}$$

At high temperatures, where the non-parabolic heavy hole band contributes to the electronic transport properties, this relation might be interrupted slightly. This rough estimation has been

shown to be reasonably consistent with a more detailed model calculation taking the band non parabolicity and multiband conduction effects into account [4].

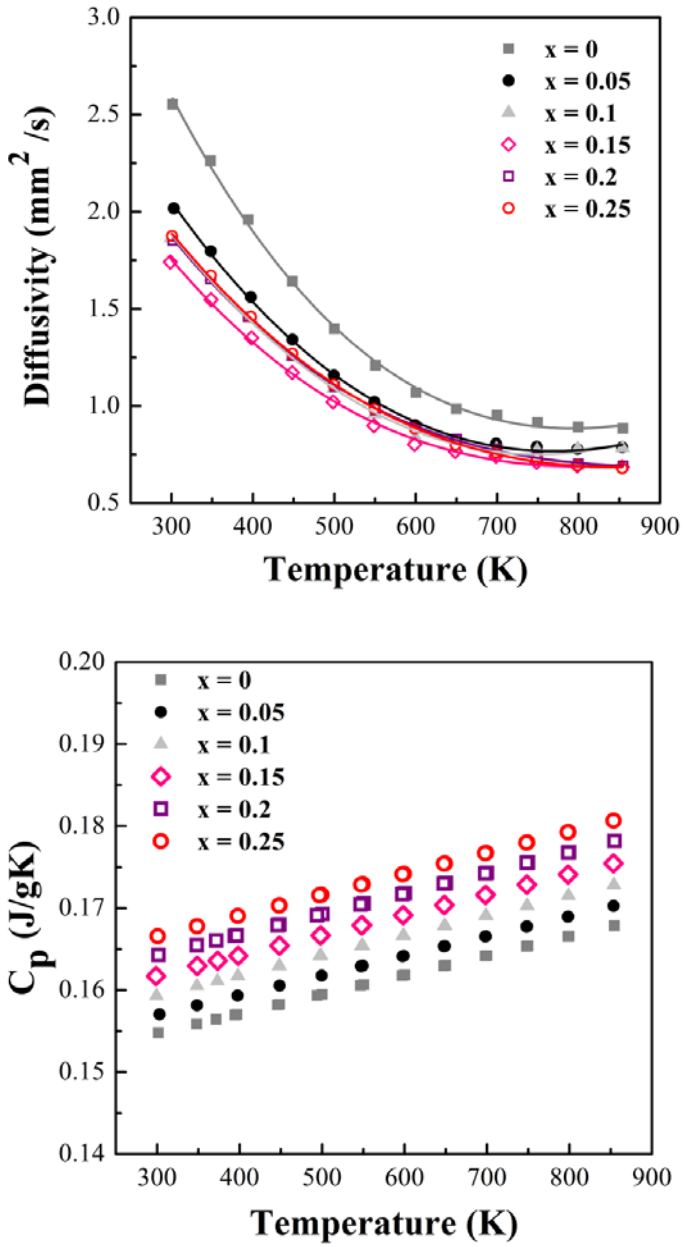

Figure S6: Temperature dependence of (a) Measured thermal diffusivity, D_T, (mm^2/s);(b) calculated Heat capacity, Cp (J/gK), of $Pb_{0.98}Na_{0.02}S_xSe_{0.1}Te_{(1-x)}$ (x = 0, 0.05, 0.1, 0.15, 0.2 and 0.25) sintered bulk sample

Reference

[1] A. Volykhov, L. Yashina, V. Shtanov, Inorg. Mater. 2006, 42, 596.
[2] A. S. Pashinkin, M. S. Mikhailova, A. S. Malkova, V. A. Fedorov, Inorg. Mater. 2009, 45, 1226.
[3] A. F. May, E. S. Toberer, A. Saramat, G. J. Snyder, Phys. Rev. B 2009, 80, 125205.
[4] Y. Pei, X. Shi, A. LaLonde, H. Wang, L. Chen, G. J. Snyder, Nature 2011, 473, 66.